ISSN 0036-0244, Russian Journal of Physical Chemistry A, 2024, Vol. 98, No. 14, pp. 3454–3466. © Pleiades Publishing, Ltd., 2024.

XXIV INTERNATIONAL CONFERENCE ON CHEMICAL THERMODYNAMICS IN RUSSIA (RCCT-2024)

# High Temperature Mass Spectrometric Study of Vaporization and Thermodynamic Properties in the $Cs_2O$–$Al_2O_3$ System

**V. A. Vorozhtcov[a,b,*] (ORCID: 0000-0002-6931-1865), V. L. Stolyarova[a,b] (ORCID: 0000-0001-7798-4405), A. L. Shilov[a,b] (ORCID: 0000-0002-2386-9759), A. V. Fedorova[a] (ORCID: 0000-0001-8242-5608), S. I. Lopatin[a,b] (ORCID: 0000-0002-6060-5349), S. M. Shugurov[a] (ORCID: 0000-0002-3075-7229), V. A. Stolyarov[a] (ORCID: 0009-0003-4505-5486), and M. E. Pavelina[a] (ORCID: 0009-0009-6176-1421)**

[a] *St. Petersburg State University, St. Petersburg, 199034 Russia*

[b] *Institute of Silicate Chemistry of Russian Academy of Sciences, St. Petersburg, 199034 Russia*

***** *e-mail: v.vorozhcov@rambler.ru*

Received August 20, 2024; revised September 10, 2024; accepted September 13, 2024

**Abstract**—Using the Knudsen effusion mass spectrometric method in the temperature range 1100–1520 K, the vaporization processes and thermodynamic properties in the $Cs_2O$–$Al_2O_3$ system were studied. The data on the component activities were fitted using the Redlich–Kister polynomial to calculate the excess Gibbs energies in this system for the first time. Thermodynamic properties found in the $Cs_2O$–$Al_2O_3$ system were discussed in the frame of the generalized lattice theory of associated solutions. It was found that the Cs–O–Al bonds made the most valuable contribution to the negative deviations from the ideality in the $Cs_2O$–$Al_2O_3$ system at the temperature 1200 K.

**Keywords:** Knudsen effusion mass spectrometry, thermodynamic properties, vaporization, modeling, cesium oxide, alumina

**DOI:** 10.1134/S0036024424703035

## INTRODUCTION

Ceramics and melts based on the $Cs_2O$–$Al_2O_3$ system are known to take part or occur in various important high temperature processes and applications [1–5]. Odoj and Hilpert [1] studied the vaporization processes of ceramics based on the $Cs_2O$–$Al_2O_3$–$SiO_2$ system with the aim to determine the potential of the compounds in this system for retention of cesium, which is of crucial importance in the nuclear technology both for operation of the fuel elements in presence of fission products and for immobilization of spent nuclear fuel. Hilpert et al. [2] showed that adding alumina and silica to the $UO_2$ particles increased the retention of cesium in the nuclear fuel unless glassy phases accompanied the formation of cesium aluminosilicates. To avoid formation of cesium-containing glasses, it was recommended to increase the $Al_2O_3$ amount and lower the $SiO_2$ content to bind cesium in the $Cs_2O$–$Al_2O_3$–$SiO_2$ ceramics. Solomah et al. [3] as well as Petrov et al. [5] pointed out that the mineral-like matrices made of alumina and titania allow for efficient disposal of radioactive wastes by incorporating and immobilizing radioactive cesium and its decay product barium in the crystal structure. Van Hoek et al. [4] mentioned that the $Cs_2O$–$Al_2O_3$ system can serve as a base for advanced materials in thermionic energy converters and in closed-cycle magneto hydrodynamic generators. It was shown that alumina ceramics is the most suitable material to be used in the construction of nuclear thermionic converter devices that are to be operated under a severely corrosive environment in presence of cesium vapor [6, 7].

Despite significant importance of the $Cs_2O$–$Al_2O_3$ system for development of modern materials science, the physicochemical properties of this system remain largely unstudied, probably due to difficulties in the sample synthesis. On many occasions, this resulted in a situation when properties of multicomponent systems involving cesium and aluminum oxides as components were studied significantly better than the corresponding characteristics of the $Cs_2O$–$Al_2O_3$ system.

Few data on the phase equilibria of the $Cs_2O$–$Al_2O_3$ system have been reported in the literature. The only studies on the phase diagram of the binary $Cs_2O$–$Al_2O_3$ system were carried out by Langlet [8] and Semenov et al. [9]. Two compounds were confirmed in the system under consideration: $Cs_2O{\cdot}Al_2O_3$, which was stable up to 973 K, with thermal decomposition or vaporization occuring at higher temperatures, and $Cs_2O{\cdot}11Al_2O_3$ with the stability range up to the temperature 1323 K [8]. Semenov et al. [9] investigated glass formation in the $Cs_2O$–$Al_2O_3$ system and man-

aged to obtain only the glass containing 60 wt % of $Cs_2O$ and 39 wt % of $Al_2O_3$.

The complete phase diagram of the $Cs_2O$–$Al_2O_3$ system is not available. However, to obtain the most general understanding of what it can look like, one can consider the phase diagram of the $K_2O$–$Al_2O_3$ system [10] since potassium and cesium are analogous alkali metals. In the $K_2O$–$Al_2O_3$ system, three compounds were identified: $KAlO_2$, $KAl_{5.5}O_{8.75}$, and $KAl_{11}O_{17}$ [10]. The $KAlO_2$ melting temperature was found to be 2508 K while the eutectic temperature between $KAlO_2$ and $KAl_{11}O_{17}$ was 2192 K [10]. Therefore, this temperature is the minimal one at which the melt appears in the concentration range $KAlO_2$–$Al_2O_3$ and, analogously, can be regarded as such in the range $CsAlO_2$–$Al_2O_3$ of the $Cs_2O$–$Al_2O_3$ system.

It should be mentioned that more information on the physicochemical properties, including phase equilibria, is available for multicomponent systems involving the binary $Cs_2O$–$Al_2O_3$ system, such as $Cs_2O$–$Al_2O_3$–$TiO_2$ system [3, 11], CaO–$Cs_2O$–$Al_2O_3$ system [4], $Cs_2O$-$Al_2O_3$–$SiO_2$ system [1, 2, 12, 13], and BaO–$Cs_2O$–$Al_2O_3$–$TiO_2$ system [5]. The vaporization processes were studied earlier in the $Cs_2O$–$Al_2O_3$–$SiO_2$ [1, 2] and $Cs_2O$–$Al_2O_3$–$TiO_2$ [3] systems. However, information on the vaporization of the $Cs_2O$–$Al_2O_3$ system has not been reported so far. So, it may be helpful for the further consideration to outline the data available on the vaporization processes of the pure oxides.

Unfortunately, there are scarce data in the literature on vaporization of pure cesium oxide. This is explained by high reactivity of cesium oxide towards oxygen, water, and carbon dioxide, which complicates synthesis of $Cs_2O$ as a pure compound. Klemm and Scharf [14] studied the vaporization processes of $Cs_2O$ using only the effusion data based on the composition of the sublimate obtained as a result of the $Cs_2O$ vaporization in vacuum. They found that the $Cs_2O$ vaporization processes depended on temperature and proposed the following reactions for the $Cs_2O$ vaporization above 623 and above 723 K, respectively [14]:

$$[Cs_2O] = (Cs_2O), \quad (1)$$

$$2[Cs_2O] = [Cs_2O_2] + 2(Cs), \quad (2)$$

where brackets correspond to the condensed phase, and parentheses correspond to the gaseous phase.

Finally, above 773 K, $Cs_2O_2$ vaporized in vacuum at a constant temperature leaving no residue [14]. However, Klemm and Scharf [14] emphasized that further studies with a mass spectrometric analysis of the vapor composition over $Cs_2O$ were necessary.

A brief account of the other studies devoted to the pure $Cs_2O$ vaporization was given elsewhere by Stolyarova et al. [15]. It was found that $Cs_2O$ vaporizes primarily with dissociation into Cs and $O_2$ according to:

$$[Cs_2O] = 2(Cs) + 0.5(O_2). \quad (3)$$

Since temperature dependences of the partial pressures of the vapor species over $Cs_2O$ had not been experimentally studied earlier, in the present study it was decided to calculate the partial pressures of the atomic cesium over pure $Cs_2O$, $p°$(Cs, Pa) in the temperature range 900–1300 K using the thermodynamic data compiled by Gurvich et al. [16] in assumption that $Cs_2O$ vaporizes according to Eq. (3):

$$\log p°(Cs, Pa) = -\frac{5825}{T} + 5.57. \quad (4)$$

Thus, it follows from the literature outline that the physicochemical properties of the $Cs_2O$–$Al_2O_3$ system have not been studied earlier despite the facts that the system under consideration is a part of many materials of great practical importance, especially in high temperature technologies, and that several multicomponent systems containing the $Cs_2O$–$Al_2O_3$ system have been examined to a certain extent. Therefore, the main goal of the present study is to investigate the vaporization processes and thermodynamic properties of the ceramics based on the $Cs_2O$–$Al_2O_3$ system at high temperatures by the Knudsen effusion mass spectrometric (KEMS) method, including the vapor composition, partial pressures of the vapor species over the samples, the component activities, and integral thermodynamic functions of the system.

## EXPERIMENTAL

### *Sample Synthesis and Characterization*

The sample of the $Cs_2O$–$Al_2O_3$ system containing 33 mol % of $Cs_2O$ was synthesized by the conventional solid-state method. Cesium carbonate $Cs_2CO_3$ and low-temperature modification of alumina $\gamma$-$Al_2O_3$ were used as the starting reagents. Cesium carbonate was initially heated at the temperature of 1073 K for 12 h. The low-temperature alumina modification $\gamma$-$Al_2O_3$ was obtained by thermal decomposition of aluminum nitrate nonahydrate at the temperature of 573 K. Then, the mixture of $Cs_2CO_3$ and $\gamma$-$Al_2O_3$ was ground in an agate mortar for 1 h. Because of the $Cs_2CO_3$ hygroscopicity, grinding of the starting reagents was carried out in the isopropyl alcohol medium. The powder obtained was pressed into pellets using a manual press mould made of organic glass. The pellets were subjected to a thermal treatment in corundum crucibles at 973 K for 365 h.

The sample of the $Cs_2O$–$Al_2O_3$ system containing 20 mol % of $Cs_2O$ was synthesized by the glycine-nitrate method [17]. As the starting reagents, $Cs_2CO_3$

**Table 1.** The chemical and phase compositions of the samples in the $Cs_2O$–$Al_2O_3$ system

| Sample | Oxide content, mol % | | | | | | Phase composition |
|---|---|---|---|---|---|---|---|
| | by synthesis | | XRFA[a] | | EPMA[a] | | |
| | $Cs_2O$ | $Al_2O_3$ | $Cs_2O$ | $Al_2O_3$ | $Cs_2O$ | $Al_2O_3$ | |
| 1 | 33.3 | 66.7 | 33.3 ± 0.4 | 66.7 ± 0.2 | 32.9 ± 0.2 | 67.1 ± 0.2 | $Al(OH)_3$, γ-$Al_2O_3$, $CsAlO_2$ |
| 2 | 20.0 | 80.0 | 19.6 ± 0.2 | 80.4 ± 0.3 | 19.4 ± 0.3 | 80.6 ± 0.3 | $Al(OH)_3$, α-$Al_2O_3$, $Cs_2(Al_2O(OH)_6)$ |

[a] XRFA is X-ray fluorescence analysis, EPMA is electron probe microanalysis.

and aluminum nitrate nonahydrate were used. The required amounts of the regents were dissolved in a dilute solution of nitric acid heated constantly using a sand bath. After complete dissolution of the reagents, glycine $C_2H_5NO_2$ was added to the solution in the mole ratio $n_{Cs_2CO_3} : n_{Al(NO_3)_3 \cdot 9H_2O} : n_{C_2H_5NO_2} = 1.0 : 8.1 : 17.2$. Evaporation of the solvent led to formation of a gel and its subsequent combustion. The obtained residue was fine white powder, which was pressed into pellets using a manual press mould made of organic glass and heated in corundum crucibles at 973 K for 870 h.

The elemental compositions of the samples were established by X-ray fluorescence analysis using an EDX 800 HS energy dispersive X-ray spectrometer (Shimadzu Corporation, Analytical and Measuring Instruments Division, Tokyo, Japan) (Table 1). Analysis was carried out in vacuum in the spectral range of characteristic emission lines of elements from carbon to uranium.

The phases formed in the samples after the synthesis were characterized by X-ray phase analysis using an Ultima IV automated multipurpose X-ray diffractometer (Rigaku Corporation, Tokyo, Japan) with copper anode ($CuK_{\alpha 1,2}$ radiation) operating at a voltage of 40 kV. Analysis of the X-ray diffraction patterns was performed with the ICDD PDF-2/Release 2011 and ICDD PDF-2/Release 2016 databases (International Centre for Diffraction Data, Newtown Square, Pennsylvania, USA).

The results of the phase composition determination are presented in Table 1. X-ray diffraction analysis of sample 1 showed presence of amorphous and crystalline phases. The main diffraction maxima were observed in the range of diffraction peaks of crystalline gibbsite $Al(OH)_3$ (14: *P*121/*n*1, ICDD PDF-2 Release 2020 RDB, 00-033-0018), γ-$Al_2O_3$ (227: *Fd*-3*m* ICDD PDF-2 Release 2016 RDB, 00-047-1292), and cesium monoaluminate $CsAlO_2$ (227: *Fd*-3*m*, ICDD PDF-2 Release 2016 RDB, 01-074-2291).

In the X-ray diffraction pattern of sample 2, the main diffraction maxima corresponded to the crystalline structure of $Al(OH)_3$ (14: *P*121/*n*1, ICDD PDF-2/Release 2011, 01-080-7022). Besides this phase, the phases of triclinic $Al(OH)_3$ (2: *P*-1, ICDD PDF-2 Release 2016 RDB, 01-077-9948), corundum α-$Al_2O_3$ (167: *R*-3*c* ICDD PDF-2 Release 2016 RDB, 01-074-4582) and $Cs_2(Al_2O(OH)_6)$ (ICDD PDF-2 Release 2016 RDB, 00-036-0465) were also identified in sample 2. The presence of hydroxoforms in the phase compositions of samples 1 and 2 may be related to hygroscopicity of cesium compounds.

The samples under study were also characterized by scanning electron microscopy (SEM) using a Merlin field emission microscope (Carl Zeiss AG, Oberkochen, Germany) with the GEMINI II electron optical column and oil-free vacuum system. Detection of secondary electrons was carried out with the standard In-lens SE and SE2 detectors. Determination of the compositions of the selected points on the surfaces of the samples was performed using the additional INCA X-Act detector (Oxford Instruments plc, Abingdon, UK) for electron probe microanalysis (EPMA).

The surfaces of the samples under study are compared in the microphotographs at magnification of ×10000 presented in Fig. 1. It follows from Fig. 1b that morphology of the surface of sample 2 was not homogeneous in shape and size of crystallites and crystallites of cubic and spherical forms could be observed. The particles of sample 1 containing higher amount of $Cs_2O$ were larger. Crystallites of sample 1 did not have a pronounced habit as can be seen in Fig. 1a.

The chemical compositions of samples 1 and 2 estimated by EPMA agreed within the determination uncertainty with the results of characterization of the samples under study using the X-ray fluorescence analysis as shown in Table 1. Moreover, the component contents obtained by the chemical analysis methods corresponded to those planned by synthesis evidencing no changes in the sample compositions because of the $Cs_2O$ selective vaporization during the sample synthesis at 973 K in air for more than 360 h.

Thus, it was concluded from the abovementioned characterization results that the samples synthesized in the present study in the $Cs_2O$–$Al_2O_3$ system could be used for the further investigation by the KEMS method.

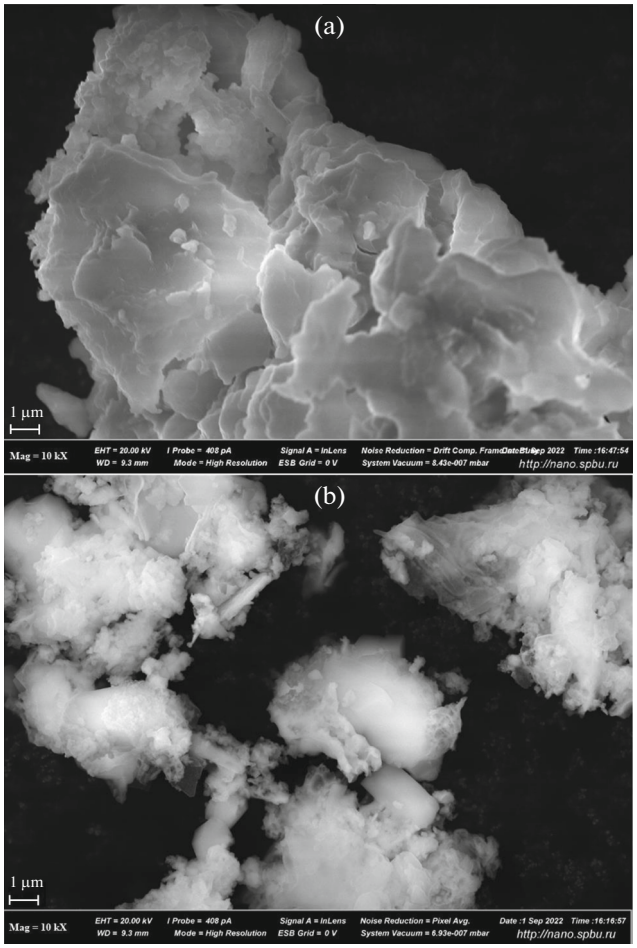


**Fig. 1.** Microphotographs of the samples in the $Cs_2O$–$Al_2O_3$ system: (a) sample 1, (b) sample 2 (according to Table 1). SEM imaging parameters were as follows: electron high tension voltage was 20 kV, microscope working distance was 9.3 mm, residual pressure was less than $10^{-4}$ Pa, in-lens detector of secondary electrons was used.

### *KEMS Method*

The Knudsen effusion mass spectrometric (KEMS) method [18, 19] performed with an MS-1301 magnetic sector mass spectrometer [20–23] (Institute of Analytical Instrumentation, St. Petersburg, Russia) was applied to study the vaporization processes and thermodynamic properties of the samples in the $Cs_2O$–$Al_2O_3$ system. The characteristics of the installation and experimental techniques were described in detail on many occasions elsewhere [15, 24, 25]. Therefore, only the most important features of the present KEMS study will be presented here.

The samples of the $Cs_2O$–$Al_2O_3$ system were vaporized from a molybdenum Knudsen effusion cell inserted in a low-temperature vaporizer. The low-temperature vaporizer of the MS-1301 mass spectrometer contains a resistance furnace with the maximum heating temperature of 1400–1600 K. The temperature of the Knudsen cell was measured by a Pt–PtRh thermocouple. The ionizing voltage used to obtain mass spectra of vapor over the samples in the effusion cell was 30 V. Calibration of the installation was carried out by the complete vaporization of CsCl and comparison of the experimental results obtained with the literature data [16].

The partial pressures of atomic cesium over the samples under study were determined by the ion current comparison method:

$$p(\mathrm{Cs}) = p(\mathrm{Ag})\frac{I(\mathrm{Cs}^+)T(\mathrm{Cs})\sigma(\mathrm{Ag})\gamma(\mathrm{Ag}^+)f(\mathrm{Ag}^+)}{I(\mathrm{Ag}^+)T(\mathrm{Ag})\sigma(\mathrm{Cs})\gamma(\mathrm{Cs}^+)f(\mathrm{Cs}^+)}, \quad (5)$$

where $p(i)$, $T(i)$, and $\sigma(i)$ are the partial pressure, the temperature, and the ionization cross-section of the vapor species $i$ over sample under study, respectively, $I(i^+)$, $\gamma(i^+)$, and $f(i^+)$ are the ion current intensity, the coefficient of the secondary electron multiplier, and the isotopic abundance, respectively, of the ion $i^+$ in the mass spectra of vapor resulting from ionization of the vapor species $i$. As shown in Eq. (5), silver was chosen as the internal vapor pressure standard in the present study, with the data on the Ag partial pressure over pure silver $p(\mathrm{Ag})$ being taken from the report by Paule and Mandel [26]. $\sigma(i)$ for Cs and Ag were taken from the technical report by Drowart et al. [19]. $\gamma(i^+)$ was considered as being inversely proportional to the square root of the ion molar mass, $M(i^+)$.

To obtain the partial pressures of oxygen $p(\mathrm{O}_2)$ over the samples in the $Cs_2O$–$Al_2O_3$ system, the Hertz–Knudsen equation modified by Zeifert [27] was used taking into account the $Cs_2O$ vaporization according to Eq. (3):

$$p(\mathrm{O}_2) = 0.25\,p(\mathrm{Cs})\sqrt{\frac{M(\mathrm{O}_2)}{M(\mathrm{Cs})}}. \quad (6)$$

Dependences of the partial pressures of the vapor species on temperature over the samples of fixed compositions are usually described by equations of the following type:

$$\log p(i) = -A/T + B, \quad (7)$$

where $A$ and $B$ are coefficients. The $A$ coefficient in Eq. (7) can be obtained in the KEMS method by measurement of the temperature dependence of the logarithm of the product of the ion current intensity in mass spectra of vapor over a sample and the temperature of the sample vaporization, $\log I(i^+)T$, because the partial pressure of vapor species in an effusion cell is known [18, 20] to be proportional to the product $I(i^+)T$:

$$p(i) = k(i)I(i^+)T, \quad (8)$$

where $k(i)$ is the mass spectrometer sensitivity coefficient.

The $B$ coefficient in Eq. (7) is obtained by determination of the absolute values of $p(i)$ over a sample under study, which was carried out in the present study using the ion current comparison method by Eq. (5).

The $Cs_2O$ activity values, $a(Cs_2O)$, in the $Cs_2O$–$Al_2O_3$ system were determined by the following equation in assumption that $Cs_2O$ and the samples of the $Cs_2O$–$Al_2O_3$ system vaporize according to Eq. (3):

$$a(Cs_2O) = \frac{p^2(Cs)p^{0.5}(O_2)}{p_o^2(Cs)p_o^{0.5}(O_2)} = \frac{p^{2.5}(Cs)}{p_o^{2.5}(Cs)}, \quad (9)$$

where the $o$ symbol corresponds to pure $Cs_2O$. The $p(Cs)$ over the samples in the $Cs_2O$–$Al_2O_3$ system and $p_o(Cs)$ over pure $Cs_2O$ were obtained by Eqs. (5) and (4).

To determine the concentration dependences of the thermodynamic properties in the $Cs_2O$–$Al_2O_3$ system, the samples based on this system were vaporized completely and ion current intensities in the mass spectra of vapor were measured over them. This allowed evaluation of the changes in the condensed phase composition of the samples because of the $Cs_2O$ selective vaporization using the complete isothermal vaporization method [28, 29].

The $Al_2O_3$ activity values in the system under consideration were calculated using the concentration dependence of the $Cs_2O$ activities that was fitted by the Redlich–Kister polynomial [30] in assumption of the continuous solid solutions in the concentration range under study:

$$\ln\frac{a(Cs_2O)}{x(Cs_2O)} = x^2(Al_2O_3)[B + C(3x(Cs_2O) - x(Al_2O_3)) + D(x(Cs_2O) - x(Al_2O_3)) \times (5x(Cs_2O) - x(Al_2O_3))], \quad (10)$$

where $x(i)$ is the mole fraction of the component $i$, $i$ = $Cs_2O$ or $Al_2O_3$, $B$, $C$, and $D$ are fitting coefficients. The values of the $B$, $C$, and $D$ coefficients were estimated by the method of least squares based on the experimental values of the $Cs_2O$ activities. Then, these values of the coefficients enabled calculation of the $Al_2O_3$ activities and excess Gibbs energies, $\Delta G^E$, by the following Redlich–Kister polynomials:

$$a(Al_2O_3) = x(Al_2O_3)\exp(x^2(Cs_2O)[B + C(x(Cs_2O) - 3(Al_2O_3)) + D(x(Cs_2O) - x(Al_2O_3)) \times (x(Cs_2O) - 5x(Al_2O_3))]), \quad (11)$$

$$\Delta G^E = RTx(Cs_2O)x(Al_2O_3)[B + C(x(Cs_2O) - x(Al_2O_3)) + D(x(Cs_2O) - x(Al_2O_3))^2]. \quad (12)$$

*Modeling Based on the Generalized Lattice Theory of the Associated Solutions*

For the further fruitful discussion of the results obtained for the first time in the $Cs_2O$–$Al_2O_3$ system, the generalized lattice theory of associated solutions (GLTAS) [31] was used. The main points of the GLTAS method [31] are as follows. Molecules of the $A$, $B$, ... types of the solution are distributed over the sites of a model lattice with a coordination number $z$, each molecule occupying $r_A$, $r_B$, ... sites. Considering the number of neighboring sites, contact points of $i$, $k$, ... types are attributed to each type of molecule. It can be shown that the number of contact points $c_A$ of molecule $A$ is related to the lattice parameters $r_A$ and $z$ as

$$c_A = r_A z - 2r_A + 2. \quad (13)$$

A pair of contact points, $i$ and $k$, belonging to molecules $A$ and $B$, respectively, represent chemical bond $A$–$B$ characterized by certain interaction energy $U_{ik}^{AB}$. Contact points are grouped into classes μ, ν ... with equal interaction energies. Let $U_{\mu\nu}^{AB}$ be a free energy of exchange of the μ-type contact point of the structural unit $A$ and ν-type contact point of the structural unit $B$ (quasi-chemical approximation). Using this notation, a system of non-linear equations for a set of unknown variables $X_\mu^A$ is written:

$$X_\mu^A \sum \eta_{\mu\nu}^{AB} X_\nu^B = Q_\mu^A x_A/2, \quad (14)$$

where $x_A$ is the mole fraction of component $A$, $Q_\mu^A$ is the number of μ-type contact points of molecule $A$, and $\eta_{\mu\nu}^{AB} \equiv \exp(-U_{\mu\nu}^{AB}/kT)$ is the corresponding energy parameter of the model (quasi-chemical approximation). The unknowns $X_\mu^A$ are auxiliary variables introduced for determination of $\eta_{\mu\nu}^{AB}$. For a particular composition and a selected set of the energy parameters $\eta_{\mu\nu}^{AB}$, the system of Eq. (14) can be solved and the values of unknowns $X_\mu^A$ can be found. Substitution of these values into equation:

$$N_{\mu\nu}^{AB} = 2X_\mu^A X_\nu^B \eta_{\mu\nu}^{AB} N, \quad [_\mu^A] \neq [_\nu^B], \quad (15)$$

where $N_{\mu\nu}^{AB}$ is the number of the μ- and ν-type contact points of the $A$ and $B$ structural units, respectively, and $N$ is the total number of structural units in the system, allows calculation of the relative numbers of bonds of different types in the model lattice.

Optimal set of the energy parameters $\eta_{\mu\nu}^{AB}$ may be determined by multiple substitution of their trial val-

**Table 2.** The Cs and $O_2$ partial vapor pressures over and the $Cs_2O$ activities in samples 1 and 2 in the $Cs_2O$–$Al_2O_3$ system

| Sample 1: $Cs_2O : Al_2O_3 = 33.3 : 66.7$, mol % | | | | Sample 2: $Cs_2O : Al_2O_3 = 20.0 : 80.0$, mol % | | | |
|---|---|---|---|---|---|---|---|
| $T$, K | $p$(Cs), Pa | $p(O_2)$, Pa | $a(Cs_2O) \times 10^4$ | $T$, K | $p$(Cs) × 10, Pa | $p(O_2) \times 10$, Pa | $a(Cs_2O) \times 10^5$ |
| 1249 | 0.51 | 0.06 | 10.2 | 1083 | 0.14 | 0.02 | 0.80 |
| 1207 | 0.19 | 0.02 | 2.23 | 1056 | 0.08 | 0.01 | 0.42 |
| 1175 | 0.07 | 0.01 | 4.50 | 1078 | 0.11 | 0.01 | 0.50 |
| 1155 | 0.04 | 0.005 | 1.68 | 1106 | 0.21 | 0.03 | 1.16 |
| 1192 | 0.09 | 0.01 | 5.42 | 1122 | 0.34 | 0.04 | 2.33 |
| 1220 | 0.20 | 0.02 | 1.93 | 1139 | 0.42 | 0.05 | 2.6 |
| 1235 | 0.26 | 0.03 | 2.58 | 1158 | 0.53 | 0.07 | 2.92 |
| 1259 | 0.48 | 0.06 | 7.15 | 1175 | 0.68 | 0.08 | 3.49 |

ues into the system of Eq. (14), obtaining the solutions $\{X_\mu^A\}$, and substituting them into equation:

$$\Delta\mu_A^E = RT\left[\sum\sum Q_\mu^A \ln(X_\mu^A/X_\mu^{Ap}/x_A) + r_A(z/2-1)\ln\left(\sum r_i x_i/r_A\right)\right], \quad (16)$$

that relates the component excess chemical potentials $\Delta\mu_i^E$ in the system under study with the model parameters. $R$ is the gas constant, $T$ is the temperature, and $X_\mu^{Ap}$ is the solution of system of equations (14) for pure component $A$. The base for optimization of the thermodynamic data is the comparison of the $\Delta\mu_i^E$ resulting from Eq. (16) with the experimental dependences.

## RESULTS

In mass spectra of the vapor over the samples 1 and 2 containing 33 and 20 mol % $Cs_2O$, only the $Cs^+$ ions were identified in the temperature range 780–1500 K. Aluminum-containing ions were observed in the mass spectra at temperatures above 2100 K. The $Cs^+$ appearance energy coincided within the determination uncertainty with the atomic cesium ionization energy of (3.9 ± 0.3) eV. This evidenced that the samples under study vaporized according to Eq. (3) in the forms of Cs and $O_2$ vapor species. The Cs and $O_2$ partial vapor pressure over and the $Cs_2O$ activities in samples 1 and 2 in the $Cs_2O$–$Al_2O_3$ system obtained according to Eqs. (5), (6), and (9) are presented in Table 2.

The temperature dependencies of the Cs partial vapor pressures over samples 1 and 2 may be represented according to Eq. (7) by the following expressions in the temperature range 1155–1259 K for sample 1:

$$\log p(\text{Cs, Pa}) = -(15400 \pm 1000)/T + (11.9 \pm 0.8) \quad (17)$$

and in the temperature range 1056–1175 K for sample 2:

$$\log p(\text{Cs, Pa}) = -(10000 \pm 400)/T + (7.4 \pm 0.4). \quad (18)$$

It should be emphasized that these data were obtained in the temperature ranges when the changes in the sample compositions during vaporization were less than one mole percent and the values of the $Cs^+$ ion current intensities during these experiments were reproduced in the frame of the traditional accuracy of the KEMS approach not exceeding 5%.

Isothermal heating of samples 1 and 2 allowed the concentration changes in the $Cs_2O$–$Al_2O_3$ system because of the $Cs_2O$ selective vaporization to be calculated using the complete isothermal vaporization method [28]. The $Cs^+$ ion current intensities in the mass spectra of the vapor over the samples were detected during the $Cs_2O$ selective vaporization as shown in Fig. 2. This led to the determination of the Cs partial vapor pressures and the $Cs_2O$ activities in the wide concentration range of the system under study.

Tables 3 and 4 represent the data on the Cs partial pressures obtained as a result of vaporization of samples 1 and 2 in the concentration ranges of the $Cs_2O$–$Al_2O_3$ system from 33.3 till 0.5 mol % $Cs_2O$ and from 20.0 till 0.1 mol % $Cs_2O$, respectively.

The $Cs_2O$ activities obtained as the temperature 1200 K as a result of studying the vaporization of samples 1 and 2 were fitted according to the Redlich–Kister polynomial [30], Eq. (10), in assumption of a con-

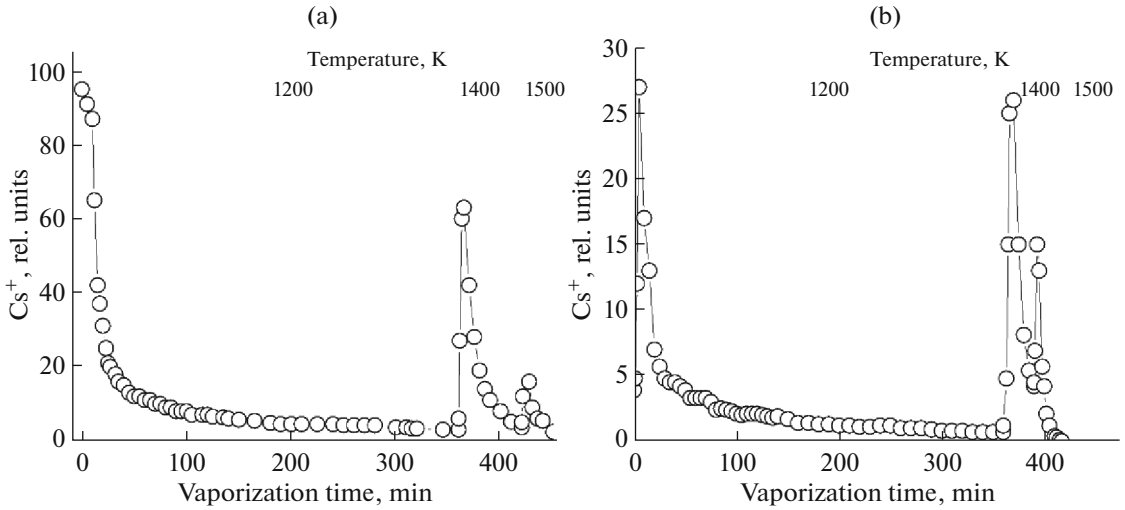


**Fig. 2.** The $Cs^+$ ion current intensities as a function of the vaporization time in mass spectrum of vapor over (a) sample 1 with the ratio of $Cs_2O : Al_2O_3 = 33.3 : 66.7$, mol %, (b) sample 2 with the ratio of $Cs_2O : Al_2O_3 = 20.0 : 80.0$, mol %.

tinuous solid solution in the concentration range of the $Cs_2O$–$Al_2O_3$ system under study. The following values of the coefficients in Eq. (10) were obtained: $B = -10.8 \pm 0.7$, $C = 42.7 \pm 2.4$, $D = 26.9 \pm 2.4$. The root mean square error of the regression was 0.52 when calculating for the natural logarithm of the $Cs_2O$ activity coefficients and $1.5 \times 10^{-5}$ when calculating for the $Cs_2O$ activities. The coefficient of determination $R^2$ was 0.99 for both $Cs_2O$ activity coefficients and activities. The obtained values of the Redlich–Kister polynomial coefficients enabled the $Al_2O_3$ activities in the $Cs_2O$–$Al_2O_3$ system to be calculated at 1200 K according to Eq. (11) as shown in Fig. 3. The component activities evidenced significant negative deviations from the ideal behavior in the $Cs_2O$–$Al_2O_3$ system at high temperatures.

## DISCUSSION

It is reasonable to discuss thermodynamic data in the $Cs_2O$–$Al_2O_3$ system found in the present study for the first time at the temperature 1200 K and higher using the GLTAS [30] statistical thermodynamic approach described above.

The obtained mass spectrometric data indicate that alumina component in the $Cs_2O$–$Al_2O_3$ system is non-volatile in the temperature range of the experiments and that the system is characterized by strong negative deviations from ideality. The uncertainty of the data for aluminum oxide that can be obtained using Gibbs–Duhem equation or Redlich–Kister polynomial increases significantly in this case since it requires extrapolation of the $Cs_2O$ activity coefficient to zero $Cs_2O$ concentration. Modeling of the thermodynamic properties of the system based on the GLTAS approach enables evaluation of the thermodynamic properties of the second component and of the system as a whole. Additionally, lattice model allows calculation of the relative number of bonds of different types.

The $Cs_2O$ activity data obtained at the temperature 1200 K by KEMS served the experimental basis for modeling and were treated as a single dataset in the optimization procedure. The concentration dependences of the component activities optimized using Eq. (16) are presented in Fig. 4. The solid and dashed

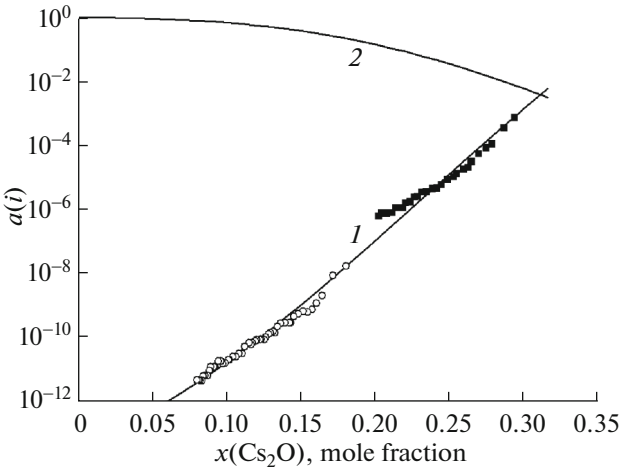


**Fig. 3.** The $Cs_2O$ (1) and $Al_2O_3$ (2) activities in the $Cs_2O$–$Al_2O_3$ system at the temperature 1200 K fitted using the Redlich–Kister polynomials, Eqs. (10) and (11), in comparison with the experimental values obtained as a result of studying the vaporization of samples 1 (■) and 2 (○).

**Table 3.** The $Cs^+$ ion current intensities, $I(Cs^+)$, in the mass spectra of the vapor and the Cs and $O_2$ partial vapor pressures, $p_i$, over sample 1 in the $Cs_2O$–$Al_2O_3$ system with the initial ratio of $Cs_2O : Al_2O_3 = 33.3 : 66.7$, mol %

| Vaporization time, min | $T$, K | $x_i$, mol % | | $I(Cs^+)$, rel. units | $p_i \times 10$, Pa | | Vaporization time, min | $T$, K | $x_i$, mol % | | $I(Cs^+)$, rel. units | $p_i \times 10$, Pa | |
|---|---|---|---|---|---|---|---|---|---|---|---|---|---|
| | | $Cs_2O$ | $Al_2O_3$ | | Cs | $O_2$ | | | $Cs_2O$ | $Al_2O_3$ | | Cs | $O_2$ |
| 0 | 1183 | 33.3 | 66.7 | 95 | 3.10 | 0.38 | 200 | 1227 | 17.7 | 82.3 | 4.5 | 0.15 | 0.02 |
| 5 | 1187 | 31.3 | 68.7 | 91 | 2.99 | 0.36 | 210 | 1228 | 17.4 | 82.0 | 4.5 | 0.15 | 0.02 |
| 10 | 1199 | 29.3 | 70.7 | 87 | 2.89 | 0.35 | 225 | 1228 | 16.9 | 83.1 | 4.5 | 0.15 | 0.02 |
| 12 | 1200 | 28.6 | 71.4 | 65 | 2.16 | 0.26 | 240 | 1228 | 16.5 | 83.5 | 4.5 | 0.15 | 0.02 |
| 15 | 1201 | 27.8 | 72.2 | 42 | 1.39 | 0.17 | 250 | 1228 | 16.2 | 83.8 | 4.2 | 0.14 | 0.02 |
| 17 | 1201 | 27.4 | 72.6 | 37 | 1.23 | 0.15 | 260 | 1228 | 15.9 | 84.1 | 4.2 | 0.14 | 0.02 |
| 20 | 1201 | 26.9 | 73.1 | 31 | 1.03 | 0.12 | 270 | 1230 | 15.6 | 84.4 | 4.2 | 0.14 | 0.02 |
| 23 | 1201 | 26.4 | 73.6 | 25 | 0.83 | 0.10 | 280 | 1232 | 15.3 | 84.7 | 4.2 | 0.14 | 0.02 |
| 25 | 1201 | 26.2 | 73.8 | 21 | 0.69 | 0.08 | 300 | 1232 | 14.8 | 85.2 | 3.6 | 0.12 | 0.02 |
| 27 | 1201 | 25.9 | 74.1 | 20 | 0.66 | 0.08 | 310 | 1233 | 14.5 | 85.5 | 3.6 | 0.12 | 0.02 |
| 32 | 1201 | 25.4 | 74.6 | 18 | 0.59 | 0.07 | 315 | 1233 | 14.4 | 85.6 | 3.3 | 0.11 | 0.01 |
| 35 | 1201 | 25.2 | 74.8 | 16 | 0.53 | 0.06 | 320 | 1233 | 14.3 | 85.7 | 3.3 | 0.11 | 0.01 |
| 40 | 1202 | 24.8 | 75.2 | 15 | 0.49 | 0.06 | 345 | 1233 | 13.7 | 86.3 | 3.0 | 0.10 | 0.01 |
| 45 | 1203 | 24.4 | 75.6 | 13 | 0.43 | 0.05 | 360 | 1233 | 13.4 | 86.6 | 3.0 | 0.10 | 0.01 |
| 50 | 1205 | 24.1 | 75.9 | 12 | 0.40 | 0.05 | 360 | 1022 | 13.4 | 86.6 | 6.0 | 0.16 | 0.02 |
| 55 | 1207 | 23.8 | 76.2 | 12 | 0.40 | 0.05 | 361 | 1349 | 13.2 | 86.8 | 27 | 1.00 | 0.12 |
| 60 | 1208 | 23.4 | 76.6 | 11 | 0.36 | 0.04 | 363 | 1370 | 12.5 | 87.5 | 60 | 2.27 | 0.28 |
| 65 | 1209 | 23.1 | 76.9 | 11 | 0.36 | 0.04 | 365 | 1380 | 11.5 | 88.5 | 63 | 2.40 | 0.29 |
| 70 | 1212 | 22.8 | 77.2 | 10 | 0.33 | 0.04 | 370 | 1389 | 9.2 | 90.8 | 42 | 1.62 | 0.19 |
| 75 | 1213 | 22.6 | 77.4 | 10 | 0.33 | 0.04 | 375 | 1399 | 7.6 | 92.4 | 28 | 1.08 | 0.13 |
| 80 | 1217 | 22.3 | 77.7 | 9.0 | 0.30 | 0.04 | 380 | 1390 | 6.5 | 93.5 | 19 | 0.73 | 0.09 |
| 85 | 1220 | 22.0 | 78.0 | 9.0 | 0.30 | 0.04 | 385 | 1392 | 5.7 | 94.3 | 14 | 0.54 | 0.06 |
| 90 | 1222 | 21.8 | 78.2 | 8.0 | 0.27 | 0.03 | 390 | 1399 | 5.1 | 94.9 | 11 | 0.42 | 0.05 |
| 95 | 1223 | 21.5 | 78.6 | 8.0 | 0.27 | 0.03 | 400 | 1399 | 4.1 | 95.9 | 8.0 | 0.31 | 0.03 |
| 100 | 1225 | 21.3 | 78.7 | 8.0 | 0.27 | 0.03 | 410 | 1388 | 3.5 | 96.5 | 5.1 | 0.19 | 0.02 |
| 105 | 1226 | 21.1 | 78.9 | 7.0 | 0.23 | 0.03 | 420 | 1389 | 3.0 | 97.0 | 3.6 | 0.13 | 0.01 |
| 115 | 1228 | 20.7 | 79.3 | 7.0 | 0.23 | 0.03 | 420 | 1419 | 3.0 | 94.0 | 5.0 | 0.19 | 0.02 |
| 120 | 1228 | 20.4 | 79.6 | 7.0 | 0.23 | 0.03 | 421 | 1455 | 2.9 | 97.1 | 12 | 0.48 | 0.05 |
| 125 | 1229 | 20.2 | 79.8 | 6.5 | 0.22 | 0.03 | 427 | 1490 | 2.0 | 98.0 | 16 | 0.66 | 0.08 |
| 135 | 1228 | 19.8 | 80.2 | 6.3 | 0.21 | 0.03 | 430 | 1490 | 1.6 | 98.4 | 9.0 | 0.39 | 0.04 |
| 140 | 1227 | 19.6 | 80.4 | 6.0 | 0.20 | 0.02 | 435 | 1488 | 1.1 | 98.9 | 6.0 | 0.24 | 0.03 |
| 150 | 1229 | 19.3 | 80.7 | 5.7 | 0.19 | 0.02 | 440 | 1501 | 0.9 | 99.1 | 5.4 | 0.22 | 0.02 |
| 165 | 1228 | 18.8 | 81.2 | 5.4 | 0.18 | 0.02 | 450 | 1502 | 0.4 | 99.6 | 2.4 | 0.10 | 0.01 |
| 180 | 1229 | 18.3 | 81.7 | 4.8 | 0.16 | 0.02 | 460 | 1502 | 0.1 | 99.9 | 1.2 | 0.05 | 0.01 |
| 190 | 1228 | 18.0 | 82.0 | 4.5 | 0.16 | 0.02 | 480 | 1502 | 0 | 100.0 | 0 | 0 | 0 |

**Table 4.** The $Cs^+$ ion current intensities, $I(Cs^+)$, in the mass spectra of the vapor and the Cs and $O_2$ partial vapor pressures, $p_i$, over sample 2 in the $Cs_2O$–$Al_2O_3$ system with the initial ratio of $Cs_2O : Al_2O_3 = 20.0 : 80.0$, mol %

| Vaporization time, min | $T$, K | $x_i$, mol % | | $I(Cs^+)$, relative units | $p_i \times 10$, Pa | | Vaporization time, min | $T$, K | $x_i$, mol % | | $I(Cs^+)$, relative units | $p_i \times 10$, Pa | |
|---|---|---|---|---|---|---|---|---|---|---|---|---|---|
| | | $Cs_2O$ | $Al_2O_3$ | | Cs | $O_2$ | | | $Cs_2O$ | $Al_2O_3$ | | Cs | $O_2$ |
| 0 | 1109 | 20.0 | 80.0 | 3.9 | 0.10 | 0.01 | 210 | 1231 | 10.1 | 89.9 | 1.2 | 0.04 | 0.004 |
| 1 | 1127 | 19.9 | 80.1 | 4.8 | 0.13 | 0.02 | 220 | 1231 | 9.9 | 90.1 | 1.1 | 0.03 | 0.004 |
| 3 | 1176 | 19.8 | 80.2 | 12 | 0.34 | 0.04 | 230 | 1234 | 9.7 | 90.3 | 1.1 | 0.03 | 0.004 |
| 5 | 1213 | 19.3 | 80.7 | 27 | 0.79 | 0.09 | 240 | 1235 | 9.6 | 90.4 | 1.2 | 0.03 | 0.004 |
| 10 | 1226 | 18.0 | 82.0 | 17 | 0.50 | 0.06 | 250 | 1235 | 9.4 | 90.6 | 1.2 | 0.03 | 0.004 |
| 15 | 1227 | 17.1 | 82.9 | 13 | 0.38 | 0.04 | 260 | 1235 | 9.2 | 90.8 | 1.0 | 0.03 | 0.004 |
| 20 | 1221 | 16.4 | 83.6 | 7.0 | 0.20 | 0.02 | 270 | 1234 | 9.1 | 90.9 | 1.0 | 0.03 | 0.004 |
| 25 | 1222 | 16.0 | 84.0 | 5.7 | 0.16 | 0.02 | 280 | 1234 | 8.9 | 91.1 | 1.0 | 0.03 | 0.004 |
| 30 | 1223 | 15.7 | 84.3 | 4.8 | 0.14 | 0.01 | 290 | 1234 | 8.8 | 91.2 | 0.9 | 0.03 | 0.003 |
| 35 | 1224 | 15.4 | 84.6 | 4.5 | 0.13 | 0.01 | 300 | 1238 | 8.7 | 91.3 | 0.8 | 0.02 | 0.003 |
| 40 | 1222 | 15.1 | 84.9 | 4.5 | 0.13 | 0.01 | 310 | 1238 | 8.5 | 91.5 | 0.8 | 0.02 | 0.003 |
| 45 | 1222 | 14.8 | 85.2 | 4.2 | 0.12 | 0.01 | 320 | 1239 | 8.4 | 91.6 | 0.8 | 0.02 | 0.003 |
| 50 | 1222 | 14.5 | 85.5 | 3.9 | 0.12 | 0.01 | 330 | 1239 | 8.3 | 91.7 | 0.7 | 0.02 | 0.003 |
| 55 | 1224 | 14.3 | 85.7 | 3.3 | 0.10 | 0.01 | 340 | 1238 | 8.2 | 91.8 | 0.7 | 0.02 | 0.003 |
| 60 | 1224 | 14.19 | 85.9 | 3.3 | 0.10 | 0.01 | 350 | 1237 | 8.1 | 91.9 | 0.7 | 0.02 | 0.002 |
| 65 | 1225 | 13.9 | 86.1 | 3.3 | 0.10 | 0.01 | 360 | 1236 | 8.0 | 92.0 | 0.7 | 0.02 | 0.002 |
| 70 | 1226 | 13.6 | 86.4 | 3.3 | 0.10 | 0.01 | 360 | 1250 | 8.0 | 92.0 | 1.2 | 0.04 | 0.004 |
| 75 | 1226 | 13.4 | 86.6 | 3.0 | 0.10 | 0.01 | 363 | 1343 | 7.8 | 92.2 | 4.8 | 0.15 | 0.02 |
| 80 | 1221 | 13.2 | 86.8 | 2.4 | 0.07 | 0.008 | 365 | 1369 | 7.5 | 92.5 | 15 | 0.50 | 0.06 |
| 85 | 1221 | 13.1 | 86.9 | 2.5 | 0.07 | 0.009 | 366 | 1391 | 7.2 | 92.8 | 25 | 0.85 | 0.10 |
| 90 | 1221 | 12.9 | 87.1 | 2.4 | 0.07 | 0.009 | 370 | 1406 | 5.6 | 94.4 | 26 | 0.89 | 0.11 |
| 95 | 1221 | 12.8 | 87.2 | 2.3 | 0.07 | 0.008 | 375 | 1412 | 3.9 | 96.1 | 15 | 0.51 | 0.06 |
| 100 | 1220 | 12.6 | 87.4 | 2.1 | 0.06 | 0.008 | 380 | 1413 | 2.9 | 97.1 | 8.1 | 0.28 | 0.03 |
| 105 | 1224 | 12.5 | 87.5 | 2.0 | 0.06 | 0.007 | 385 | 1414 | 2.4 | 97.6 | 5.4 | 0.19 | 0.02 |
| 110 | 1226 | 12.3 | 87.7 | 2.1 | 0.06 | 0.007 | 390 | 1413 | 2.0 | 98.0 | 4.2 | 0.14 | 0.02 |
| 115 | 1228 | 12.2 | 87.8 | 2.1 | 0.06 | 0.007 | 390 | 1443 | 2.0 | 98.0 | 4.5 | 0.16 | 0.02 |
| 120 | 1228 | 12.0 | 88.0 | 2.1 | 0.06 | 0.007 | 391 | 1460 | 1.9 | 98.1 | 6.9 | 0.24 | 0.03 |
| 125 | 1228 | 11.9 | 88.1 | 2.0 | 0.06 | 0.007 | 393 | 1483 | 1.5 | 98.5 | 15 | 0.54 | 0.07 |
| 130 | 1228 | 11.7 | 88.3 | 1.9 | 0.06 | 0.007 | 395 | 1499 | 1.0 | 99.0 | 13 | 0.47 | 0.06 |
| 135 | 1228 | 11.6 | 88.4 | 1.8 | 0.05 | 0.007 | 398 | 1502 | 0.5 | 99.5 | 5.7 | 0.21 | 0.03 |
| 140 | 1228 | 11.5 | 88.5 | 1.9 | 0.05 | 0.007 | 400 | 1503 | 0.3 | 99.7 | 4.2 | 0.15 | 0.02 |
| 150 | 1228 | 11.2 | 88.8 | 1.7 | 0.05 | 0.006 | 402 | 1504 | 0.2 | 99.8 | 2.1 | 0.08 | 0.01 |
| 160 | 1228 | 11.0 | 89.0 | 1.4 | 0.04 | 0.005 | 405 | 1516 | 0.1 | 99.9 | 1.2 | 0.04 | 0.005 |
| 170 | 1228 | 10.8 | 89.2 | 1.4 | 0.04 | 0.005 | 410 | 1515 | 0.1 | 99.9 | 0.4 | 0.01 | 0.002 |
| 180 | 1230 | 10.6 | 89.4 | 1.3 | 0.04 | 0.005 | 412 | 1513 | 0.1 | 99.9 | 0.3 | 0.01 | 0.001 |
| 190 | 1231 | 10.4 | 89.6 | 1.3 | 0.04 | 0.005 | 415 | 1525 | 0.1 | 99.9 | 0.1 | 0.004 | $4.6 \times 10^{-4}$ |
| 200 | 1231 | 10.2 | 89.8 | 1.2 | 0.04 | 0.004 | 417 | 1524 | 0 | 100 | 0 | 0 | 0 |

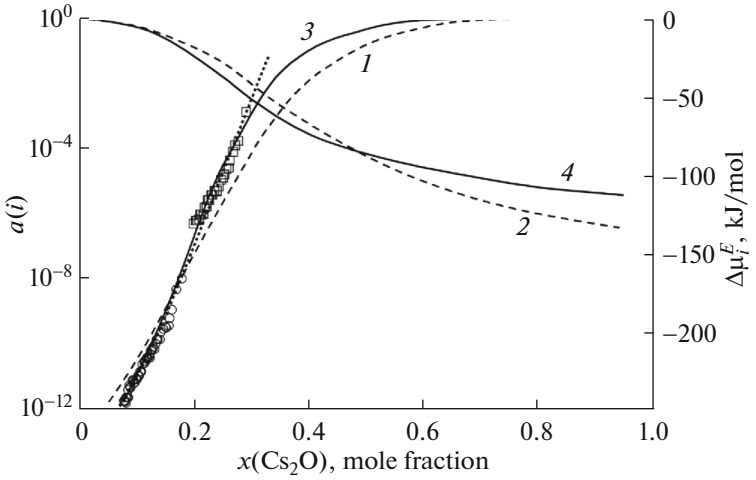


**Fig. 4.** Thermodynamic activities and excess chemical potentials of (*1*, *3*) $Cs_2O$ and (*2*, *4*) $Al_2O_3$ in the $Cs_2O$–$Al_2O_3$ system at 1200 K simulated within the GLTAS approach. The experimental values in the plot are marked by □ and ○ for the samples containing 33.3 and 20.0 mol % $Cs_2O$, respectively. Dotted curve shows the results of the Redlich–Kister approximation.

curves in the figure are the results of calculations for two different sets of model parameters.

Originally [31], the theory was developed for organic solutions in which the relative molar volumes of components can be accurately expressed by the number $r$ of sites occupied by the components in the model lattice [32]. When the theory is applied to inorganic oxide systems, the parameters used for modeling are usually near their minimal possible values ($z = 3$, $r = 1–2$) and therefore the choice of the lattice model satisfying Eq. (13) is rather limited.

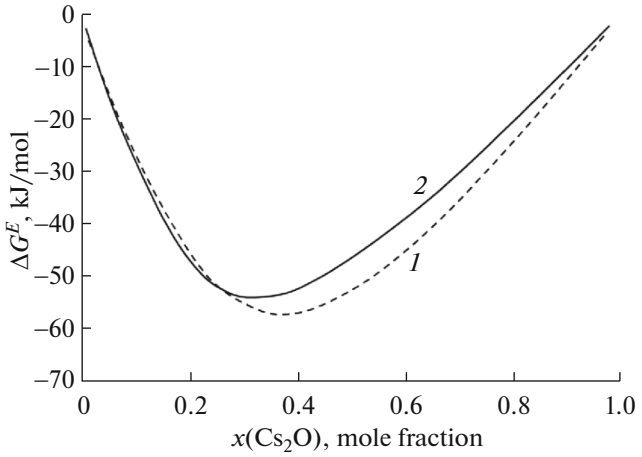


**Fig. 5.** The excess Gibbs energy in the $Cs_2O$–$Al_2O_3$ system at 1200 K optimized within the GLTAS approach using the experimental data on the $Cs_2O$ activity. (*1*) Values calculated using equal energies of the Cs–O[Al] and Al–O[Cs] bonds and (*2*) the results when the energies of the Cs–O[Al] and Al–O[Cs] bonds were treated as independent adjustable parameters.

To make the modeling method more flexible, it is slightly modified in the present study. The number of contact points assigned to the structural units is increased, allowing a more accurate account for the molar volumes of the components, the ratio of which in the $Cs_2O$–$Al_2O_3$ system is 2.53. A model lattice with the coordination number 4 is chosen, each $Cs_2O$ structural unit occupying 3 sites of the lattice and $Al_2O_3$ occupying 1 site. $Cs_2O$ is assigned 2 cesium-type contact points of the first type, 2 cesium-type contact points of the second type (denoted in the text below as Cs and Cs', respectively), and 2 oxygen-type contact points. $Al_2O_3$ has 2 aluminum- and 2 oxygen-type contact points. The interaction energies of the Cs–Cs, Al–Al, and O–O pairs are set zero.

Hence, the adjustable energy parameters corresponding to Cs–O[Cs], Cs'–O[Cs], Cs–O[Al], and Cs'–O[Al] bonds, where in brackets the atom of the second coordination sphere is indicated, were considered in the computations. Moreover, two approaches to considering the Cs–O[Al] bond were employed. In the first approach, the Cs–O[Al] bond was not differentiated. In the second version of the modeling, the Cs–O[Al] and Al–O[Cs] bonds were treated as independent adjustable parameters. The energy parameter for Al–O–Al bond was determined in our earlier study as a result of optimization of the $Al_2O_3$–$SiO_2$–$ZrO_2$ system [21].

The GLTAS optimization of the experimental thermodynamic data resulted in the concentration dependences of the excess Gibbs energy (Fig. 5) and the relative numbers of bonds of different types in the model lattice (Fig. 6) in the $Cs_2O$–$Al_2O_3$ system.

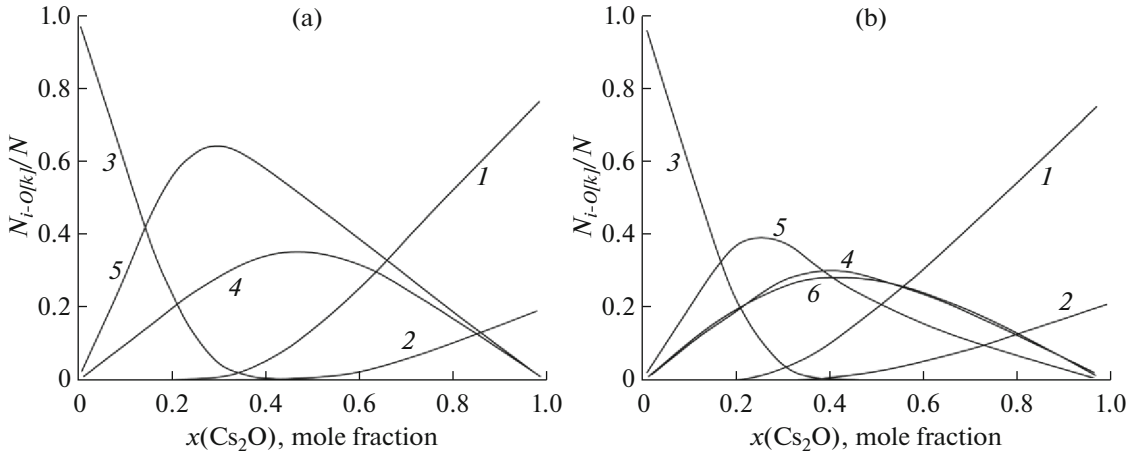


**Fig. 6.** Relative numbers $N_{i\text{-}O[kj]}/N$ of bonds in the $Cs_2O$–$Al_2O_3$ system calculated using the GLTAS approach. Atoms of the second coordination sphere in the bonds under consideration are indicated in brackets: (*1*) Cs–O[Cs], (*2*) Cs'–O[Cs], (*3*) Al–O[Al], (*4*) Cs–O[Al], (*5*) Cs'–O[Al], (*6*) Al–O[Cs]. The energy parameters of the Cs–O[Al] and Al–O[Cs] bonds were considered (a) equal and (b) as the independent adjustable variables.

If the volumes of the A and B structural units in a binary system A–B do not differ greatly, they occupy an equal number of sites in the model lattice, the difference in the energies of the A–O[B] and B–O[A] bonds does not affect the results of optimization since only their sum is the actual input parameter in the calculations. For the model lattice of the $Cs_2O$–$Al_2O_3$ system in which the numbers of sites occupied by the components are related as 3 : 1, a much better agreement between the modeling and experimental results can be expected if the Cs–O[Al] and Al–O[Cs] bonds are assigned separate adjustable energy parameters. The results of such computations are shown in Figs. 4 and 5 (solid curves). The concentration dependence of the $Cs_2O$ activities simulated by assuming different energy parameters of the Cs–O[Al] and Al–O[Cs] bonds (curve *3* in Fig. 4) demonstrates a nearly perfect approximation of the experimental data, which is close to that of the Redlich–Kister polynomial and is superior to the simpler model with no differentiation of the Cs–O[Al] bond (curve *1* in Fig. 4). The data obtained show that the interaction energies of Cs in real structures of the solutions in the $Cs_2O$–$Al_2O_3$ system are spread over the energy range of 1–2 kJ/mol at temperatures about 1200 K. Thus, it may be concluded that the modified version of the model with additional contact points and bonds in the lattice is justified and can be further developed.

The obtained results confirm that the systems with very strong deviations of the thermodynamic properties from ideality can be adequately described within the framework of the GLTAS model. The observed shift of the minimum of the curve in Fig. 5 and maxima of the curves *4*–*6* in Fig. 6 towards compositions enriched with $Al_2O_3$ can be explained largely by the difference in the molar volumes of the components and the corresponding coordination numbers of the components in the lattice. Since the molar volume of $Cs_2O$ is much larger than that of $Al_2O_3$, the relative number of mixed bonds in Fig. 6 reaches its maximum at lower concentrations of cesium oxide.

## CONCLUSIONS

This study is the first where the vaporization processes and thermodynamic properties of the $Cs_2O$–$Al_2O_3$ system were examined by the Knudsen effusion mass spectrometric method. The vapor composition, the partial pressures of the vapor species, and the $Cs_2O$ activities in the system under consideration were determined experimentally in the temperature range 1100–1520 K, demonstrating significant negative deviations from the ideal behavior. The $Al_2O_3$ activities and excess Gibbs energies were calculated at 1200 K using the Redlich–Kister polynomial and based on the generalized lattice theory of associated solutions, which illustrated the correlation between the deviations of the thermodynamic properties from the ideality and the concentration dependences of the relative numbers of bonds of various types formed in the model lattice when the second coordination sphere is taken into account. The partial pressures of the vapor species over the samples of the $Cs_2O$–$Al_2O_3$ system may be of interest for the further development of the materials based on this system, including their synthesis by the vapor deposition techniques. Thermodynamic data obtained in the present study in the $Cs_2O$–$Al_2O_3$ system using the Knudsen effusion mass spectrometric method in the temperature range

1100–1520 K may be successfully used in the further modeling of the multicomponent systems that are of importance for nuclear applications based on the CALPHAD approach.

## ACKNOWLEDGMENTS

Identification of the samples under study was performed using the equipment of the Research Park of St. Petersburg State University: X-ray fluorescent analysis in the Centre for Innovative Technologies of Composite Nanomaterials, X-ray phase analysis in the Research Centre for X-ray Diffraction Studies, as well as scanning electron microscopy and electron probe microanalysis in the Interdisciplinary Resource Centre for Nanotechnology. The authors are grateful to the Cryogenic Department of the Research Park of St. Petersburg State University for the uninterrupted supplies of liquid nitrogen for the mass spectrometer.

## FUNDING

This study was carried out with the financial support of the Ministry of Science and Higher Education of the Russian Federation according to the research project "Physicochemical description of high temperature processes in multicomponent systems for the extraction and disposal of cesium and strontium at elimination of consequences of severe accidents on nuclear power plants (INES-7)" (project no. 075-15-2021-1383).

## CONFLICT OF INTEREST

The authors of this work declare that they have no conflicts of interest.

## REFERENCES

1. R. Odoj and K. Hilpert, Zeitschr. Naturforsch., A **35**, 9 (1980). https://doi.org/10.1515/ZNA-1980-0103
2. K. Hilpert, R. Odoj, and H. W. Nürnberg, Nucl. Technol. **61**, 71 (1983). https://doi.org/10.13182/NT83-A33144
3. A. G. Solomah, R. Odoj, and C. Freiburg, J. Am. Ceram. Soc. **67**, 50 (1984). https://doi.org/10.1111/J.1151-2916.1984.TB19754.X
4. J. A. M. van Hoek, F. J. J. van Loo, L. R. Wolff, and R. Metselaar, J. Eur. Ceram. Soc. **5**, 93 (1989). https://doi.org/10.1016/0955-2219(89)90015-0
5. S. A. Petrov, L. F. Grigor'eva, O. Y. Sinel'shchikova, et al., Glass Phys. Chem. **29**, 316 (2003). https://doi.org/10.1023/A:1024498418871
6. R. G. Smith, F. Hargreaves, G. T. J. Mayo, and A. G. Thomas, J. Nucl. Mater. **10**, 191 (1963). https://doi.org/10.1016/0022-3115(63)90054-0
7. F. Hargreaves, G. T. J. Mayo, and A. G. Thomas, J. Nucl. Mater. **18**, 212 (1966). https://doi.org/10.1016/0022-3115(66)90084-5
8. G. Langlet, Ph.D. Thesis (Univ. Paris, Gif-sur-Yvette, 1969). http://inis.iaea.org/Search/search.aspx?orig_q=RN:36007943. Accessed September 15, 2024.
9. N. N. Semenov, Izv. Sib. Otd. Akad. Nauk SSSR, Ser. Khim. Nauk **152**, 148 (1969).
10. D. G. Kim, E. Moosavi-Khoonsari, and I. H. Jung, J. Eur. Ceram. Soc. **38**, 3188 (2018). https://doi.org/10.1016/J.JEURCERAMSOC.2018.02.030
11. J. D. Groeneveld, M. Burianek, J. Birkenstock, et al., Zeitschr. Krist - Cryst. Mater. **235**, 533 (2020). https://doi.org/10.1515/ZKRI-2020-0056
12. T. V. Solov'eva, G. A. Vydrik, and I. K. Moroz, Russ. J. Inorg. Chem. **15**, 1771 (1970).
13. M. Fisch, T. Armbruster, and B. Kolesov, J. Solid State Chem. **181**, 423 (2008). https://doi.org/10.1016/J.JSSC.2007.12.014
14. W. Klemm and H.-J. Scharf, Zeitschr. Anorg. Allgem. Chem. **303**, 263 (1960). https://doi.org/10.1002/ZAAC.19603030505
15. V. L. Stolyarova, V. A. Vorozhtcov, S. I. Lopatin, et al., Rapid Commun. Mass Spectrom. **35**, e9097 (2021). https://doi.org/10.1002/RCM.9097
16. L. V. Gurvich, I. V. Veitz, V. A. Medvedev, et al., *Thermodynamic Properties of Individual Substances* (Nauka, Moscow, 1982), Vol. 4, Nos. 1–2 [in Russian].
17. A. V. Fedorova, V. A. Stolyarov, M. E. Pavelina, et al., Russ. J. Inorg. Chem. **68**, 911 (2023). https://doi.org/10.1134/S0036023623600909
18. K. Hilpert, Rapid Commun. Mass Spectrom. **5**, 175 (1991). https://doi.org/10.1002/rcm.1290050408
19. J. Drowart, C. Chatillon, J. Hastie, and D. Bonnell, Pure Appl. Chem. **77**, 683 (2005). https://doi.org/10.1351/pac200577040683
20. V. L. Stolyarova and G. A. Semenov, *Mass Spectrometric Study of the Vaporization of Oxide Systems* (Wiley, Chichester, 1994).
21. V. L. Stolyarova, A. L. Shilov, S. I. Lopatin, et al., Commun. Mass Spectrom. **37**, e9433 (2023). https://doi.org/10.1002/rcm.9433
22. S. I. Lopatin, S. M. Shugurov, Z. G. Tyurnina, and N. G. Tyurnina, Glass Phys. Chem. **47**, 38 (2021). https://doi.org/10.1134/S1087659621010077
23. S. I. Lopatin, Glass Phys. Chem. **48**, 117 (2022). https://doi.org/10.1134/S1087659622020055
24. V. A. Vorozhtcov, V. L. Stolyarova, S. I. Lopatin, et al., Rapid Commun. Mass Spectrom. **31**, 111 (2017). https://doi.org/10.1002/rcm.7764
25. V. L. Stolyarova, V. A. Vorozhtcov, S. I. Lopatin, et al., Rapid Commun. Mass Spectrom. **35**, e9079 (2021). https://doi.org/10.1002/RCM.9079
26. R. C. Paule and J. Mandel, Pure Appl. Chem. **31**, 395 (1972). https://doi.org/10.1351/pac197231030395

27. P. L. Zeifert, in *High Temperature Technology* (Wiley, New York, 1956), p. 485.

28. L. N. Sidorov and V. B. Shol'ts, Int. J. Mass Spectrom. Ion Phys. **8**, 437 (1972). https://doi.org/10.1016/0020-7381(72)80014-7

29. L. N. Sidorov and P. A. Akishin, Dokl. Akad. Nauk SSSR **151**, 136 (1963).

30. O. Redlich and A. T. Kister, Ind. Eng. Chem. **40**, 345 (1948). https://doi.org/10.1021/ie50458a036

31. J. A. Barker, J. Chem. Phys. **20**, 1526 (1952). https://doi.org/10.1063/1.1700209

32. L. M. Krutynina and N. A. Smirnova, Russ. J. Phys. Chem. **47**, 2782 (1973).